THE MOMENT OF INERTIA OF PROTO-NEUTRON STAR PSR J0740+6620

Xian-Feng Zhao, Zhen-Hai Wu

School of Sciences, Southwest Petroleum University, Chengdu 610500, China

Received 18 February 2022, accepted 13 June 2022, published online 14 July 2022

The effect of nucleon coupling constants on the moment of inertia of proto-neutron star (PNS) PSR J0740+6620 is examined with relativistic mean-field theory in consideration of a baryon octet. Here, nucleon coupling parameters DD-MEI, NL1, NL2, TW99, and GM1 are used. Under the constraints of the observed mass $M = 2.05$–$2.24\ M_{\odot}$ of PNS PSR J0740+6620 (taking the observed mass of neutron star (NS) PSR J0740+6620), the radius of the PNS calculated by us with GM1 is the smallest, $R = 14.63$–13.44 km, while the radius calculated with TW99 is the largest, $R = 17.46$–17.07 km. The radii calculated from the other three sets of nucleon coupling parameters are between the two values mentioned above. The maximum value of the moment of inertia calculated with the nucleon coupling parameters TW99, NL1, DD-MEI, NL2, and GM1 decreases in turn. Under the constraint of the observed mass of PNS PSR J0740+6620 (taking the observed mass of NS PSR J0740+6620), the moment of inertia calculated with NL1, NL2, DD-MEI, and TW99 increases with the increase of the central energy density and mass, and decreases with the increase of the radius. The moment of inertia calculated with GM1 decreases with the increase of central energy density and mass, and increases with the increase of the radius. The moment of inertia of the PNS PSR J0740+6620 calculated by us with five groups of nucleon coupling parameters is between 2.465×10^{45}–2.050×10^{45} g cm^2 (GM1) and 3.597×10^{45}–3.883×10^{45} g cm^2 (TW99).

DOI:10.5506/APhysPolB.53.8-A1

1. Introduction

Neutron stars (NSs) are dense, rapidly rotating objects [1–4]. In the later stages of stellar evolution, a proto-neutron star (PNS) is formed in the core by a supernova explosion and an NS is formed by neutrino radiation, which gradually cools down [5]. The structure of a PNS depends more sensitively on the composition of the star than on its entropy and the number of trapped neutrinos plays an important role in determining of the composition [6].

If nucleons, hyperons, and leptons are present in the stellar core, the finite-temperature Brueckner–Bethe–Goldstone method shows that both finite-temperature and neutrino capture reduce the maximum mass value of purely nucleonic stars. For supersonic stars, the effect is reversed, as neutrino capture converts the presence of hyperons into a larger baryon density, thus greatly strengthening the equation of state (EoS) [7, 8]. The structure of the PNS will affect its mass and radius [9, 10].

The mass and radius of the PNS are closely related to its moment of inertia, which is an important physical quantity to describe the rotational properties of PNS. Due to the large mass of PNSs, the effect of general relativity must be taken into account when calculating their moment of inertia [11, 12].

In recent years, a series of massive NSs (NS PSR J1614-2230, $M = 1.97 \pm 0.04\ M_{\odot}$(2010) [13], then $M = 1.93 \pm 0.07\ M_{\odot}$(2016) [14]; NS PSR J0348+0432, $M = 2.01 \pm 0.04\ M_{\odot}$(2013) [15]; NS PSR J0740+6620, $M = 2.14^{+0.10}_{-0.09}\ M_{\odot}$(2020) [16]) have been discovered. The mass, radius, and moment of inertia of the PNSs of these massive NSs are important for describing their rotational properties and the evolution of stars, which are of great interest to us.

The relativistic mean-field (RMF) theory is a theory that describes finite nuclei [17] and has been successful in describing NS matter [18, 19]. The results show that the transition density of hyperon stars is sensitive to the nucleon coupling parameters [4]. The transformation of an NS into a hyperon star means that a large number of nucleons in the NS become hyperons. The composition of the particles in an NS will affect its mass and radius [18]. Thus, the mass and radius of the NS (and, by extension, the moment of inertia) are also sensitive to the nucleon coupling parameters.

In this work, the effect of nucleon coupling constants on the moment of inertia of PNS PSR J0740+6620 is studied by using the RMF theory in consideration of a baryon octet.

2. RMF theory of PNS matter

Considering the interactions between nucleons and hyperons, the Lagrangian density of hadron matter containing mesons $f_0(975)$ (denoted as σ^*) and $\phi(1020)$ (denoted as ϕ) [20] reads as follows [19]:

$$\begin{aligned}\mathcal{L} \;=\; & \sum_B \bar{\Psi}_B \Big(i\gamma_\mu \partial^\mu - m_B + g_{\sigma B}\sigma + g_{\sigma^* B}\sigma^* \\ & - g_{\omega B}\gamma_\mu \omega^\mu - g_{\phi B}\gamma_\mu \phi^\mu - \frac{1}{2} g_{\rho B}\gamma_\mu \tau\, \rho^\mu \Big) \Psi_B \\ & + \frac{1}{2}\left(\partial_\mu \sigma \partial^\mu \sigma - m_\sigma^2 \sigma^2\right) - \frac{1}{3} g_2 \sigma^3 - \frac{1}{4} g_3 \sigma^4\end{aligned}$$

$$
\begin{aligned}
&+\frac{1}{2}m_{\omega}^{2}\omega_{\mu}\omega^{\mu}+\frac{1}{2}m_{\rho}^{2}\rho_{\mu}\,\rho^{\mu}\\
&+\frac{1}{2}\left(\partial_{\mu}\sigma^{*}\partial^{\mu}\sigma^{*}-m_{\sigma^{*}}^{2}\sigma^{*2}\right)+\frac{1}{2}m_{\phi}^{2}\phi_{\mu}\phi^{\mu}\\
&+\sum_{\lambda=e,\mu}\bar{\Psi}_{\lambda}\left(i\gamma_{\mu}\partial^{\mu}-m_{\lambda}\right)\Psi_{\lambda}\,. \qquad (1)
\end{aligned}
$$

Given the neutrino binding, the partition function of baryon of the PNS matter is

$$
\begin{aligned}
\ln Z_{B} \;=\; & \frac{V}{T}\langle\mathcal{L}\rangle+\sum_{B}\frac{2J_{B}+1}{2\pi^{2}}\\
&\times\int_{0}^{\infty}k^{2}\mathrm{d}k\left\{\ln\left[1+\mathrm{e}^{-(\varepsilon_{B}(k)-\mu_{B})/T}\right]\right\}. \qquad (2)
\end{aligned}
$$

Here, k is the Fermi momentum of baryon B.

The total baryon number density [9, 10] is obtained from above

$$
\rho=\sum_{B}\frac{2J_{B}+1}{2\pi^{2}}b_{B}\int_{0}^{\infty}k^{2}n_{B}(k)\mathrm{d}k\,. \qquad (3)
$$

After applying the RMF approximation, the energy density and the pressure [9, 10] respectively are

$$
\begin{aligned}
\varepsilon \;=\; & \frac{1}{2}m_{\sigma}^{2}\sigma^{2}+\frac{1}{2}m_{\sigma^{*}}^{2}\sigma^{*2}+\frac{1}{3}g_{2}\sigma^{3}+\frac{1}{4}g_{3}\sigma^{4}\\
&+\frac{1}{2}m_{\omega}^{2}\omega_{0}^{2}+\frac{1}{2}m_{\phi}^{2}\phi^{2}+\frac{1}{2}m_{\rho}^{2}\rho_{03}^{2}\\
&+\sum_{B}\frac{2J_{B}+1}{2\pi^{2}}\int_{0}^{\infty}k^{2}n_{B}(k)\mathrm{d}k\sqrt{k^{2}+m_{B}^{*2}}\,, \qquad (4)\\
p \;=\; & -\frac{1}{2}m_{\sigma}^{2}\sigma^{2}-\frac{1}{2}m_{\sigma^{*}}^{2}\sigma^{*2}-\frac{1}{3}g_{2}\sigma^{3}-\frac{1}{4}g_{3}\sigma^{4}\\
&+\frac{1}{2}m_{\omega}^{2}\omega_{0}^{2}+\frac{1}{2}m_{\phi}^{2}\phi^{2}+\frac{1}{2}m_{\rho}^{2}\rho_{03}^{2}\\
&+\frac{1}{3}\sum_{B}\frac{2J_{B}+1}{2\pi^{2}}\int_{0}^{\infty}\frac{k^{4}}{\sqrt{k^{2}+m_{B}^{*2}}}n_{B}(k)\mathrm{d}k\,. \qquad (5)
\end{aligned}
$$

Here, $n_B(k)$ is the Fermi–Dirac distribution function of baryon

$$
n_{B}(k)=\frac{1}{1+\exp\left[\left(\varepsilon_{B}(k)-\mu_{B}\right)/T\right]}\,. \qquad (6)
$$

Ignoring the interactions of leptons at finite temperature, their partition function is written as

$$\ln Z_L = \frac{V}{T}\sum_i \frac{\mu_i^4}{24\pi^2}\left[1+2\left(\frac{\pi T}{\mu_i}\right)^2+\frac{7}{15}\left(\frac{\pi T}{\mu_i}\right)^4\right] + V\sum_\lambda \frac{1}{\pi^2}\int_0^\infty k^2 \mathrm{d}k \left\{\ln\left[1+\mathrm{e}^{-(\varepsilon_\lambda(k)-\mu_\lambda)/T}\right]\right\}. \tag{7}$$

The first line represents the contribution of massless neutrinos and the second line the contribution of electrons and μs.

The lepton number density is

$$\rho_l = \frac{1}{\pi^2}\int_0^\infty k^2 n_l(k)\mathrm{d}k\,, \tag{8}$$

$$\rho_\nu = \frac{\pi^2 T^2\mu_\nu+\mu_\nu^3}{6\pi^2}\,, \tag{9}$$

where l stands for electron e, and μ and ν stand for electron neutrino and μ neutrino, respectively.

The contribution of leptons to the energy density and the pressure is

$$\varepsilon = \sum_l \frac{1}{\pi^2}\int_0^\infty k^2 n_l(k)\mathrm{d}k\sqrt{k^2+m_l^2} + \sum_\nu\left(\frac{7\pi^2T^4}{120}+\frac{T^2\mu_\nu^2}{4}+\frac{\mu_\nu^4}{8\pi^2}\right), \tag{10}$$

$$p = \frac{1}{3}\sum_l \frac{1}{\pi^2}\int_0^\infty \frac{k^4}{\sqrt{k^2+m_l^2}} n_l(k)\mathrm{d}k + \sum_\nu \frac{1}{360}\left(7\pi^2T^4+30T^2\mu_\nu^2+\frac{15\mu_\nu^4}{\pi^2}\right). \tag{11}$$

The chemical potentials of baryons are

$$\mu_i = \mu_n - q_i\left(\mu_e-\mu_{\nu e}\right). \tag{12}$$

To describe the neutrino trapping, the content of lepton in PNS is defined as

$$Y_{l\nu} = Y_l + Y_\nu = \frac{\rho_l+\rho_\nu}{\rho}\,, \tag{13}$$

where $Y_{l\nu}$ represents the content of electrons, μ, electron neutrinos, and μ neutrinos, Y_l represents the content of electrons and μs, and Y_ν represents the content of electron neutrinos and μ neutrinos. Due to electron neutrino confinement, the threshold for the occurrence of μ particles increases, so it can be assumed that $Y_\mu = 0$. The electron content is desirable $Y_e = 0.1$–0.4 [6, 21, 22]. However, neutrino binding is not considered in this work.

We obtain the mass and the radius of a PNS by the Tolman–Oppenheimer–Volkoff (TOV) equation [23, 24]

$$\frac{\mathrm{d}p}{\mathrm{d}r} = -\frac{(p+\varepsilon)\left(M+4\pi r^3 p\right)}{r\left(r-2M\right)}, \tag{14}$$

$$M = 4\pi \int_0^R \varepsilon r^2 \mathrm{d}r\,. \tag{15}$$

The moment of inertia of a slowly rotating PNS is given by [11, 12]

$$I = \frac{8\pi}{3}\int_0^R \mathrm{d}r r^4 \frac{\varepsilon + p}{\sqrt{1-2M(r)/r}} \frac{[\Omega - \omega(r)]}{\Omega} \mathrm{e}^{-\nu}\,. \tag{16}$$

Here, ν is given by

$$-\frac{\mathrm{d}\nu(r)}{\mathrm{d}r} = \frac{1}{\varepsilon + p}\frac{\mathrm{d}p}{\mathrm{d}r}, \tag{17}$$

and the angular velocity is given by

$$-\frac{1}{r^4}\frac{\mathrm{d}}{\mathrm{d}r}\left(r^4 j \frac{\mathrm{d}\bar{\omega}}{\mathrm{d}r}\right) + \frac{4}{r}\frac{\mathrm{d}j}{\mathrm{d}r}\bar{\omega} = 0\,. \tag{18}$$

The $j(r)$ is

$$j(r) = \mathrm{e}^{-(\nu+\lambda)} = \mathrm{e}^{-\nu}\sqrt{1-2M(r)/r}\,, \qquad r < R\,. \tag{19}$$

The boundary condition are given by

$$\frac{\mathrm{d}\bar{\omega}}{\mathrm{d}r}_{|r=0} = 0\,, \tag{20}$$

$$\nu\left(\infty\right) = 0\,, \tag{21}$$

$$\bar{\omega}\left(R\right) = \Omega - \frac{R}{3}\frac{\mathrm{d}\bar{\omega}}{\mathrm{d}r}_{|r=R}\,. \tag{22}$$

3. Parameters

Here, PNS matter is calculated by 10 sets of nucleon coupling parameters (DD-MEI [25], GL85 [18], GL97 [19], NL1 [26], NL2 [26], TW99 [25], GM1 [27], FSUGold [28], FSU2R [29], and FSU2H [29]).

We define the ratios of hyperon coupling constant to nucleon coupling constant as $x_{\sigma h} = \frac{g_{\sigma h}}{g_\sigma} = x_\sigma$, $x_{\omega h} = \frac{g_{\omega h}}{g_\omega} = x_\omega$, $x_{\rho h} = \frac{g_{\rho h}}{g_\rho}$ (h denoting hyperons Λ, Σ, and Ξ), which are in the range of $\sim 1/3$ to 1 [27].

We select $x_{\rho h}$s by SU(6) symmetry [30, 31]. For the maximum mass of the PNS increasing with the increase of parameters $x_{\sigma h}$ and $x_{\omega h}$ [32], we should take the largest possible $x_{\omega h}$ to obtain the largest possible mass of the PNS. We choose $x_{\omega h} = 0.9$ and $x_{\sigma h}$ is derived by equation as follows [19]:

$$U_h^{(N)} = m_n \left(\frac{m_n^*}{m_n} - 1 \right) x_{\sigma h} + \left(\frac{g_\omega}{m_\omega} \right)^2 \rho_0 x_{\omega h} \,. \tag{23}$$

Here, we select the hyperon-potentials as $U_\Lambda^{(N)} = -30$ MeV [31, 33, 34], $U_\Sigma^{(N)} = 30$ MeV [31, 33–35], and $U_\Xi^{(N)} = -14$ MeV [36], respectively.

The parameters of the mesons σ^* and ϕ coupling to hyperons can be chosen as [20]

$$g_{\phi\Xi} = 2g_{\phi\Lambda} = 2g_{\phi\Sigma} = \frac{-2\sqrt{2}g_\omega}{3} \,, \tag{24}$$

$$g_{\sigma^*\Lambda}/g_\sigma = g_{\sigma^*\Sigma}/g_\sigma = 0.69 \,, \tag{25}$$

$$g_{\sigma^*\Xi}/g_\sigma = 1.25 \,. \tag{26}$$

We take the temperature of PNS PSR J0740+6620 as $T = 20$ MeV [5].

Figure 1 and Table 1 show the mass and radius of the PNS calculated by us with the above 10 sets of nucleon coupling parameters. It can be seen that only the nucleon coupling parameters DD-MEI, NL1, NL2, TW99, and GM1 can give the mass of the PNS PSR J0740+6620. In this paper, we study the influence of nucleon coupling parameters DD-MEI, NL1, NL2, TW99, and GM1 on the moment of inertia of PNS PSR J0740+6620.

4. Radius of PNS PSR J0740+6620

The observed mass of PNS PSR J0740+6620 is $M = 2.05$–$2.24\ M_\odot$ [16], corresponding to that for which the radius calculated by us with GM1 is the smallest, $R = 14.63$–13.44 km, while the radius calculated by us with TW99 is the largest, $R = 17.46$–17.07 km (see Fig. 1 and Table 1). The radii calculated by us from the other three sets of nucleon coupling parameters are between the two above values.

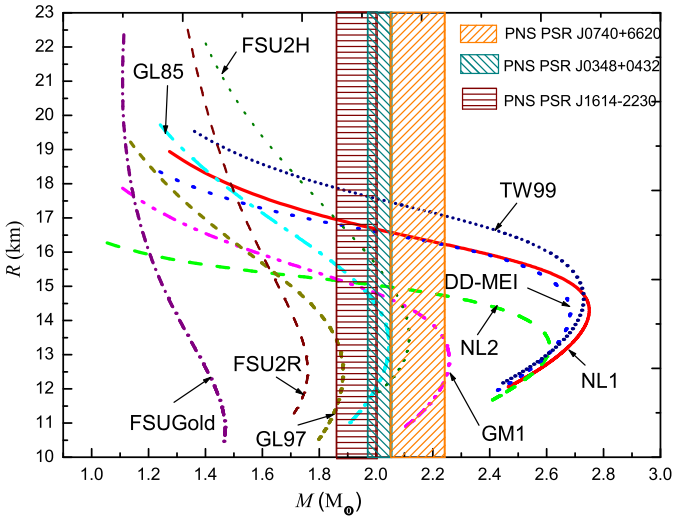

Fig. 1. The radius of the PNS calculated by us as a function of the mass. The shaded areas show the mass ranges of PNS J1614-2230, PNS J0348+0432, and PNS PSR J0740+6620, respectively.

Table 1. Results of the PNS PSR J0740+6620 calculated by us in this work. The mass of PNS PSR J0740+6620 is $M = 2.05$–$2.24\ M_\odot$. R, ρ_c, ε_c, p_c, and I are the radius, the central baryon density, the central energy density, the central pressure, and the moment of inertia of PNS PSR J0740+6620, respectively.

Parameter	R	ρ_c	ε_c	p_c	I
unit	[km]	[fm^{-3}]	$\times 10^{15}$ g cm^{-3}	$\times 10^{35}$ dyne cm^{-2}	$\times 10^{45}$ g cm^2
NL1	16.59–16.23	0.336–0.365	0.609–0.672	1.043–1.375	3.381–3.715
NL2	14.98–14.73	0.394–0.439	0.712–0.812	1.328–1.818	3.061–3.238
DD–MEI	16.52–16.20	0.328–0.361	0.594–0.666	0.996–1.312	3.428–3.705
TW99	17.46–17.07	0.303–0.333	0.552–0.617	0.869–1.138	3.597–3.883
GM1	14.63–13.44	0.512–0.737	0.976–1.546	1.960–4.363	2.465–2.050

At the center of the PNS, the baryon density reaches its maximum, known as the central baryon density (expressed as ρ_c). The central baryon densities of PNSs calculated by us with different nucleon coupling parameters are different. The central baryon density of PNS PSR J0740+6620 calculated by us with GM1 is the highest, *i.e.* $\rho_c = 0.512$–0.737 fm^{-3}, and that calculated with TW99 is the lowest, *i.e.* $\rho_c = 0.303$–0.333 fm^{-3}. The central baryon density of the PNS PSR J0740+6620 calculated with other nucleon coupling parameters is between the two.

5. Energy density and pressure of PNS PSR J0740+6620

Figure 2 shows the pressure p of PNS PSR J0740+6620 calculated by us with different nucleon coupling constants as a function of energy density ε. Each curve terminates at its central baryon density ρ_c.

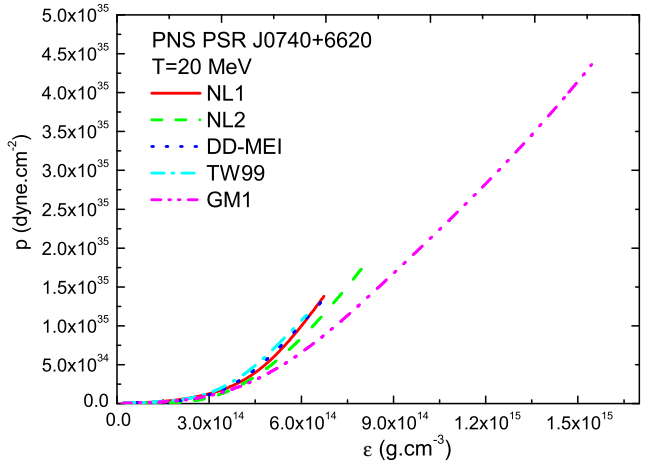

Fig. 2. The pressure p of PNS PSR J0740+6620 calculated by different nucleon coupling constants as a function of energy density ε. Each curve terminates at its central baryon density ρ_c.

As can be seen from Fig. 2, the pressure p of the PNS increases with the increase of energy density ε. For the same energy density ε, the pressure p calculated by us with TW99 is the maximum, and that calculated with GM1 is the minimum. The calculated pressures with DD-MEI, NL1, and NL2 are in between and decrease successively.

The energy density and pressure at the center of the PNS are the greatest, known as the central energy density and the central pressure (denoted ε_c and p_c, respectively). It can also be seen from Fig. 2 and Table 1 that the central energy density ε_c and central pressure p_c of PNS PSR J0740+6620 calculated by us with different nucleon coupling parameters are different, and some of them are significantly different. The central energy density ε_c and central pressure p_c of PNS PSR J0740+6620 calculated by us with TW99, DD-MEI, NL1, NL2, and GM1 increase successively.

6. Effect of nucleon coupling constants on moment of inertia of PNS PSR J0740+6620

The moment of inertia I and the mass M of the PNS calculated by us with five nucleon coupling constants as a function of central energy density are shown in Fig. 3.

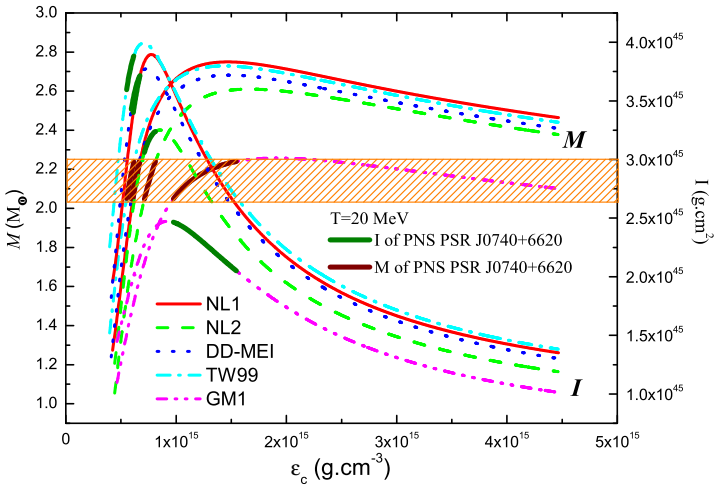

Fig. 3. The moment of inertia I and the mass M of the PNS calculated by five nucleon coupling constants as a function of central energy density. The thick solid lines represent the calculated moment of inertia of PNS PSR J0740+6620.

As can be seen from Fig. 3, the moment of inertia I of the PNS first increases with the increase of the central energy density ε_c, and then decreases with the increase of the central energy density ε_c after reaching a peak value. The peaks of the moment of inertia calculated by us with the nucleon coupling parameters TW99, NL1, DD-MEI, NL2, and GM1 decrease in turn.

The thick solid lines in Fig. 3 represent the calculated moment of inertia I and mass M of PNS PSR J0740+6620. As can be seen from Fig. 3, the moment of inertia I of the PNS PSR J0740+6620 calculated by us with the nuclear coupling parameters TW99, NL1, DD-MEI, and NL2 increases with the increase of the central energy density ε_c, while that calculated with GM1 decreases with the increase of the central energy density ε_c. This is because, despite the limitation of the observed mass of the PNS PSR J0740+6620, the mass of the PNS calculated by us with the five groups of nucleon coupling parameters increases with the increase of the central energy density (the amplitude of mass increase is the same), and the radius decreases with the increase of the central energy density. However, the radius reduction calculated with NL1, NL2, DD-MEI, and TW99 is less than that calculated with GM1 (see Fig. 4). Therefore, the moment of inertia calculated from NL1, NL2, DD-MEI, and TW99 increases with the increase of central energy density, while that calculated from GM1 decreases with the increase of central energy density.

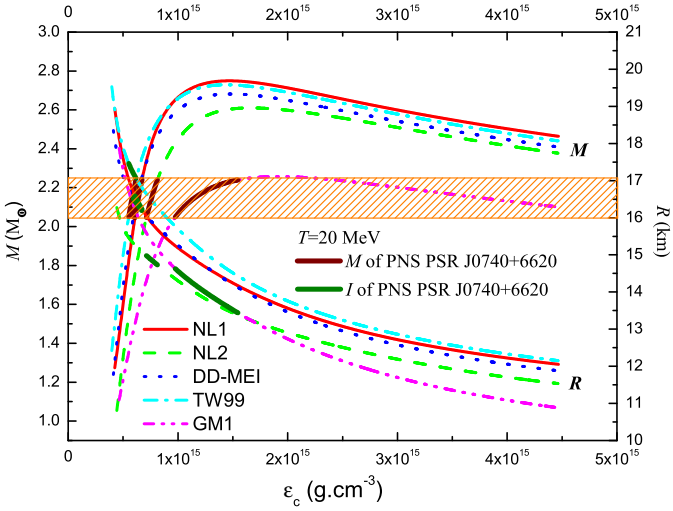

Fig. 4. The mass and radius of the PNS as a function of central energy density ε_c. The thick solid lines represent the mass and radius of PNS PSR J0740+6620.

Figure 5 shows the moment of inertia of the PNS as a function of mass. Here, the thick solid lines represent the moment of inertia of PNS PSR J0740+6620. It can be seen from the figure that the moment of inertia of the PNS first increases with the increase of its mass, and then decreases with the increase of its mass after reaching the maximum moment of inertia. When the maximum mass of the PNS is exceeded, the moment of inertia decreases with the decrease of the mass.

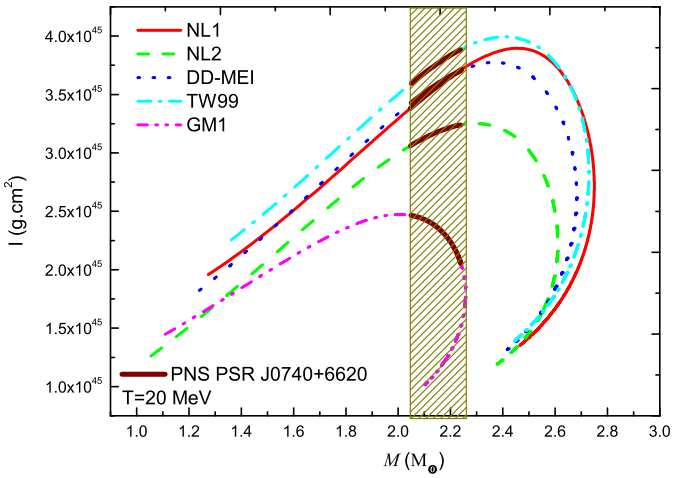

Fig. 5. The moment of inertia of the PNS as a function of mass. The thick solid lines represent the moment of inertia of PNS PSR J0740+6620.

For the PNS PSR J0740+6620, the moment of inertia calculated by us from NL1, NL2, DD-MEI, and TW99 increases with the increase of mass, while those calculated by us from GM1 decrease as the mass increases. The reason is the same as the case that under the constraint of the observation mass of PNS PSR J0740+6620, the radius decrease of the PNS calculated with GM1 is greater than that calculated with NL1, NL2, DD-MEI, and TW99.

The moment of inertia of the PNS as a function of the radius is shown in Fig. 6. The moment of inertia of the PNS first increases with the increase of the radius. After reaching the peak, it decreases with the increase of the radius. Under the constraint of the observation mass of the PNS PSR J0740+6620, the relationship between moment of inertia and radius calculated with different nucleon coupling parameters is different. The moment of inertia of the PNS PSR J0740+6620 calculated with NL1, NL2, DD-MEI, and TW99 decreases with the increase of radius, while the moment of inertia calculated with GM1 increases with the increase of radius.

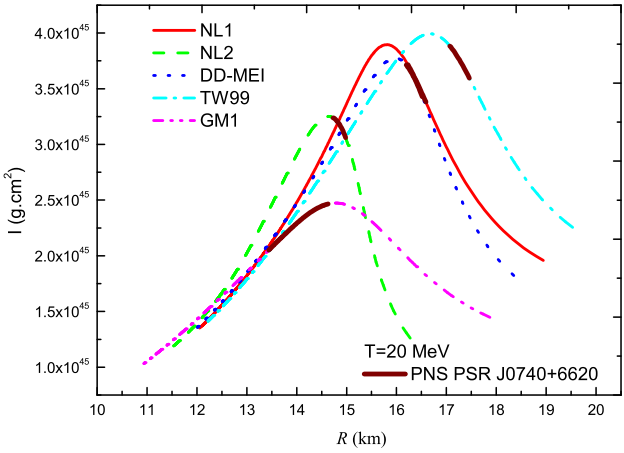

Fig. 6. The moment of inertia of the PNS as a function of the radius. The thick solid lines represent the mass and radius of PNS PSR J0740+6620.

It can be seen from Table 1 that the moment of inertia of the PNS PSR J0740+6620 calculated with five groups of nucleon coupling parameters is between 2.465×10^{45}–2.050×10^{45} g cm^2 (GM1) and 3.597×10^{45}–3.883×10^{45} g cm^2 (TW99).

7. Summary

The effect of nucleon coupling constants on the moment of inertia of PNS PSR J0740+6620 is examined with the RMF theory in consideration of a baryon octet. In this work, nucleon coupling parameters DD-MEI, NL1, NL2, TW99, and GM1 are used.

Under the constraints of the observed mass $M = 2.05$–$2.24\ M_\odot$ of PNS PSR J0740+6620, the radius of the PNS calculated by us with GM1 is the smallest, $R = 14.63$–13.44 km, while the radius calculated by us with TW99 is the largest, $R = 17.46$–17.07 km. The radii calculated by us from the other three sets of nucleon coupling parameters are between the two above values. The central baryon densities of PNSs calculated with different nucleon coupling parameters are different. The central baryon density of PNS PSR J0740+6620 calculated with GM1 is the highest, *i.e.* $\rho_c = 0.512$–$0.737\ \mathrm{fm}^{-3}$, while that calculated with TW99 is the lowest, *i.e.* $\rho_c = 0.303$–$0.333\ \mathrm{fm}^{-3}$, and those calculated with other nucleon coupling parameters are between the two.

For the same energy density ε, the pressure p calculated by us with TW99 is the maximum, and that calculated by us with GM1 is the minimum. The calculated pressures with DD-MEI, NL1, and NL2 are in between and decrease successively. The central energy density ε_c and central pressure p_c of PNS PSR J0740+6620 calculated with different nucleon coupling parameters are different, and some of them are significantly different. The central energy density ε_c and central pressure p_c of PNS PSR J0740+6620 calculated with TW99, DD-MEI, NL1, NL2, and GM1 increase successively.

The maximum value of the moment of inertia calculated by us with the nucleon coupling parameters TW99, NL1, DD-MEI, NL2, and GM1 decrease in turn. Under the constraint of the observed mass of PNS PSR J0740+6620 (taking the observed mass of NS PSR J0740+6620), the mass of the PNS calculated with the five groups of nucleon coupling parameters increases with the increase of the central energy density, and the calculated radius of the PNS decreases with the increase of the central energy density (the radius calculated by GM1 decreases the most). These lead to the following results: under the constraint of the observed mass of PNS PSR J0740+6620 (taking the observed mass of NS PSR J0740+6620), the moment of inertia calculated with NL1, NL2, DD-MEI, and TW99 increases with the increase of the central energy density and mass, and decreases with the increase of the radius. The moment of inertia calculated by us with GM1 decreases with the increase of central energy density and mass, and increases with the increase of radius. The moment of inertia of the PNS PSR J0740+6620 calculated by us from five groups of nucleon coupling parameters is between 2.465×10^{45}–$2.050 \times 10^{45}\ \mathrm{g\,cm^2}$ (GM1) and 3.597×10^{45}–$3.883 \times 10^{45}\ \mathrm{g\,cm^2}$ (TW99).

This work was supported by the Natural Science Foundation of China (grant No. 11447003).

REFERENCES

[1] X.H. Li *et al.*, «Numerically fitting the electron Fermi energy and the electron fraction in a neutron star», *Int. J. Mod. Phys. D* **25**, 1650002 (2016).

[2] C. Zhu *et al.*, «Modified Fermi energy of electrons in a superhigh magnetic field», *Mod. Phys. Lett. A* **31**, 1650070 (2016).

[3] D.H. Wen *et al.*, «Frame Dragging Effect on Moment of Inertia and Radius of Gyration of Neutron Star», *Mod. Phys. Lett. A* **22**, 631 (2007).

[4] H.Y. Jia *et al.*, «How and When Will a Neutron Star Become a Hyperon Star?», *Chinese Phys. Lett.* **18**, 1571 (2001).

[5] A. Burrows, J.M. Lattier, «The birth of neutron stars», *Astrophys. J.* **307**, 178 (1986).

[6] M. Prakash *et al.*, «Composition and structure of protoneutron stars», *Phys. Rep.* **280**, 1 (1997).

[7] O.E. Nicotra, M. Baldo, G.F. Burgio, H.J. Schulze, «Protoneutron stars within the Brueckner–Bethe–Goldstone theory» *Astron. Astrophys.* **451**, 213 (2006).

[8] G.F. Burgio, M. Baldo, O.E. Nicotra, H.J. Schulze, «A microscopic equation of state for protoneutron stars», *Astrophys. Space Sci.* **308**, 387 (2007).

[9] N.K. Glendenning, «Finite temperature metastable matter», *Phys. Lett. B* **185**, 275 (1987).

[10] N.K. Glendenning, «Hot metastable state of abnormal matter in relativistic nuclear field theory», *Nucl. Phys. A* **469**, 600 (1987).

[11] J.B. Hartle, «Slowly Rotating Relativistic Stars. I. Equations of Structure», *Astrphys. J.* **150**, 1005 (1967).

[12] J.B. Hartle, K.S. Thorne, «Slowly Rotating Relativistic Stars. II. Models for Neutron Stars and Supermassive Stars», *Astrphys. J.* **153**, 807 (1968).

[13] P.B. Demorest *et al.*, «A two-solar-mass neutron star measured using Shapiro delay», *Nature* **467**, 1081 (2010).

[14] E. Fonseca *et al.*, «The Nanograv Nine-Year Data Set: Mass and Geometric Measurements of Binary Millisecond Pulsars», *Astrphys. J.* **832**, 167 (2016).

[15] J. Antoniadis *et al.*, «A Massive Pulsar in a Compact Relativistic Binary», *Science* **340**, (2013).

[16] H.T. Cromartie *et al.*, «Relativistic Shapiro delay measurements of an extremely massive millisecond pulsar», *Nat. Astron.* **4**, 72 (2020).

[17] S.G. Zhou, «Multidimensionally constrained covariant density functional theories — nuclear shapes and potential energy surfaces», *Phys. Scr.* **91**, 063008 (2016).

[18] N.K. Glendenning, «Neutron stars are giant hypernuclei?», *Astrphys. J.* **293**, 470 (1985).

[19] N.K. Glendenning, «Compact Stars: Nuclear Physics, Particle Physics, and General Relativity», *Springer-Verlag New York, Inc.*, New York 1997.

[20] J. Schaffner *et al.*, «Multiply Strange Nuclear Systems», *Ann. Phys.* **235**, 35 (1994).

[21] M. Kachelrieß, «Neutrino self-energy and pair creation in neutron stars», *Phys. Lett. B* **426**, 89 (1998).

[22] R. Zhou, H. Guo, «Equation of State of Dense Matter with Trapped Neutrinos», *Chinese Phys. C* **28**, 26 (2004).

[23] R.C. Tolman, «Static Solutions of Einstein's Field Equations for Spheres of Fluid», *Phys. Rev.* **55**, 364 (1939).

[24] J.R. Oppenheimer, G.M. Volkoff, «On Massive Neutron Cores», *Phys. Rev.* **55**, 374 (1939).

[25] S. Typel, H.H. Wolter, «Relativistic mean field calculations with density-dependent meson–nucleon coupling», *Nucl. Phys. A* **656**, 331 (1999).

[26] S.J. Lee *et al.*, «Relativistic Hartree Calculations for Axially Deformed Nuclei», *Phys. Rev. Lett.* **57**, 2916 (1986).

[27] N.K. Glendenning, S.A. Moszkowski, «Reconciliation of neutron-star masses and binding of the Λ in hypernuclei», *Phys. Rev. Lett.* **67**, 2414 (1991).

[28] B.G. Todd-Rutel, J. Piekarewicz, «Neutron-Rich Nuclei and Neutron Stars: A New Accurately Calibrated Interaction for the Study of Neutron-Rich Matter», *Phys. Rev. Lett.* **95**, 122501 (2005).

[29] L. Tolos, M. Centelles, A. Ramos, «The Equation of State for the Nucleonic and Hyperonic Core of Neutron Stars», *Publ. Astron. Soc. Aust.* **34**, e065 (2017).

[30] J. Schaffner, I.N. Mishustin, «Hyperon-rich matter in neutron stars», *Phys. Rev. C* **53**, 1416 (1996).

[31] J. Schaffner-Bielich, A. Gal, «Properties of strange hadronic matter in bulk and in finite systems», *Phys. Rev. C* **62**, 034311 (2000).

[32] X.F. Zhao, «The Composition of Baryon in the Proto Neutron Star PSR J0348+0432», *Int. J. Theor. Phys.* **58**, 1060 (2019).

[33] S. Weissenborn, D. Chatterjee, J. Schaffner-Bielich, «Hyperons and massive neutron stars: The role of hyperon potentials», *Nucl. Phys. A* **881**, 62 (2012).

[34] A. Gal, E.V. Hungerford, D.J. Millener, «Strangeness in nuclear physics», *Rev. Mod. Phys.* **88**, 035004 (2016).

[35] C.J. Batty, E. Friedman, A. Gal, «Strong interaction physics from hadronic atoms», *Phys. Rep.* **287**, 385 (1997).

[36] T. Harada, Y. Hirabayashi, A. Umeya, «Production of doubly strange hypernuclei via Ξ^- doorways in the $^{16}\mathrm{O}(K^-, K^+)$ reaction at 1.8 GeV/c», *Phys. Lett. B* **690**, 363 (2010).